THE JOURNAL OF PHYSICAL CHEMISTRY B
A JOURNAL OF THE AMERICAN CHEMICAL SOCIETY

pubs.acs.org/JPCB

Article

Sampling the Bulk Viscosity of Water with Molecular Dynamics Simulation in the Canonical Ensemble

René Hafner, Gabriela Guevara-Carrion, Jadran Vrabec, and Peter Klein*

Cite This: J. Phys. Chem. B 2022, 126, 10172−10184

Read Online

ACCESS | Metrics & More | Article Recommendations | Supporting Information

ABSTRACT: The bulk viscosity, a transport coefficient in the Navier−Stokes equation, is often neglected in the continuum mechanics of Newtonian fluids. Recently, however, the role of the bulk viscosity is highlighted in the area of surface and interface-related phenomena, in systematic model up-scaling and as an important quantity for the interpretation of acoustic sensor data. The prediction of the bulk viscosity usually employs molecular dynamics and the Green−Kubo linear response theory, which is used to sample transport properties in general from molecular trajectories. Since simulations are usually carried out at specified state points in concert with the evaluation of other thermodynamic properties, the role of thermostats in molecular dynamics needs to be explored systematically. In this work, we carefully investigate the role of thermostatting schemes and numerical implementations of the Green−Kubo formalism, in particular in the canonical ensemble, using two popular water force field models. It turns out that the sampling of the bulk and shear viscosities is a delicate challenge since details of thermostatting and numerical subtleties may have an influence on the results beyond statistical uncertainties. Based on the present findings, we conclude with hints on how to construct robust sampling in the canonical ensemble for the bulk viscosity.

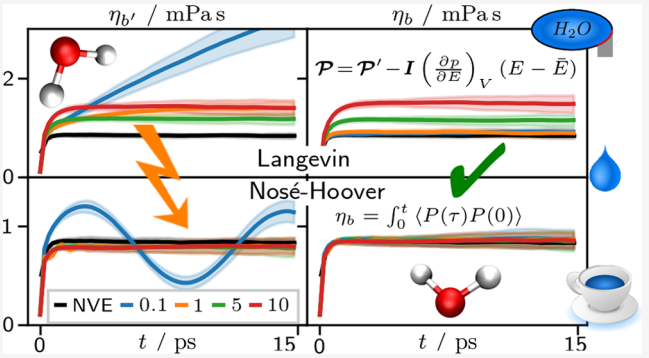

1. INTRODUCTION

Molecular dynamics (MD) simulation is a versatile tool to study structure and dynamics of systems that are relevant in physics, chemistry, biology, and engineering. In its original form, MD relies on the statistical interpretation of atomic or molecular trajectories in the microcanonical NVE ensemble obtained by numerical integration of Newton's equation of motion under the influence of their mutual interactions. Because of the energy conservation law, the NVE ensemble is most natural for MD simulations[1] and it also forms the basis of statistical thermodynamics. However, to facilitate comparisons with experiments that are usually conducted at constant temperature, volume, or pressure, isothermal ensembles, such as the canonical (NVT) or the isothermal−isobaric (NpT), are often preferred.

A large number of thermostatting algorithms for MD simulation in the NVT ensemble have been proposed.[2−6] They operate by coupling the simulated molecular system or a part of it with a heat bath. Heat exchange to maintain a constant temperature is either achieved by a modification of Newton's equation of motion or of the molecule velocities. Therefore, when using a thermostat, Newtonian dynamics is always disturbed to some extent.[7] Because of their time-dependent nature, transport properties, like diffusion coefficients, viscosities, or thermal conductivity, are expected to be affected by thermostatting. In fact, these effects may lead to spurious transport property data as described in a number of works.[1,7,8] Nevertheless, simulations in the NVT ensemble are still widely employed for sampling transport properties, not only because they do not require previous knowledge of the total energy but also because many other thermodynamic properties, like the thermodynamic factor, can be accessed simultaneously. In this case, sampling of transport properties with the NVT ensemble should be done carefully so that the induced perturbation of the molecular trajectories is sufficiently small not to introduce significant artifacts.[8]

From a computational fluid dynamics (CFD) point of view, momentum transport in a fluid is described by the Navier−Stokes equation,[9] which is a continuity equation for the momentum, whose variation over time is given by the divergence of a viscous stress tensor. In this equation, the bulk viscosity is the coefficient for hydrostatic density changes induced by the velocity field and thus is not directly related to momentum transport. Stokes[10] proposed his hypothesis in

Received: August 23, 2022
Revised: October 27, 2022
Published: November 29, 2022

https://doi.org/10.1021/acs.jpcb.2c06035
J. Phys. Chem. B 2022, 126, 10172−10184

1845 that remedies the lack of bulk viscosity data by stating that it is zero, although he knew that his assumption is insufficient. In the incompressible limit, widely assumed for many CFD problems in the low-Mach-number regime, the bulk viscosity may be safely ignored since density changes are neglected. However, in this limit, the speed of sound diverges and, consequently, this approximation does not apply to phenomena with a finite speed of sound.

On the other hand, it is well known that in macroscopic models of acoustics, the role of the bulk viscosity in entropy production and thus in wave attenuation is very important; see ref 11 for a recent review. From a phenomenological point of view, sound waves introduce small out-of-equilibrium disturbances on the molecular level by imposing variations of macroscopic properties, like pressure and density, which relax toward the equilibrium. The type of such molecular relaxation processes is not important since any relaxation process produces entropy and therefore dissipates energy. From this phenomenological point of view, internal molecular relaxation processes manifest in a nonzero bulk viscosity on the level of macroscopic transport equations. This phenomenological picture was derived for water in 1948 by Hall in ref 12, and a more general derivation from a macroscopic entropy transport equation incorporating microscopic relaxation effects can be found in ref 9.

Phenomenologically, the bulk viscosity is to be expected to be important, among others, for interface-related phenomena, like the dynamic behavior of gas bubbles in liquids and shock waves; see, e.g., ref 13 and references therein. Here, the dynamics of macroscopic variables describing the system necessarily cause out-of-equilibrium disturbances on the molecular level in small volume elements, triggering molecular relaxation processes. Furthermore, many difficulties encountered with up-scaling procedures required for coarse-graining MD models are caused by incomplete time scale separation[14] between the dynamics of the "variables of interest" and the "variables to be integrated out". As an example, thermal fluctuations of nano-objects couple to sound waves, leading to effective interactions that propagate in a compressible fluid at a finite speed of sound. Their magnitude and attenuation highly depend on the bulk viscosity.[15] Recently developed acoustic sensor concepts for monitoring liquid flow are now realized,[16] which directly measure the acoustic viscosity, a linear combination of the shear and bulk viscosities. It allows to monitor bulk flow properties, which are hard to sample with other sensor technologies.

The aim of this work is to complement literature studies[1,7,8] on the sampling of diffusion coefficients and the shear and bulk viscosities with molecular dynamics simulations. The calculation of the bulk viscosity of liquid water was investigated by employing six different thermostats. Water was chosen as a model system because it has strong intermolecular interactions and is ubiquitous in nature and technical applications. Furthermore, the shear viscosity of liquid water under ambient conditions, i.e., 298 K and 1 bar, $\eta_s = (0.888 \pm 0.01)$ mPas, is on the same order of magnitude as its bulk viscosity, $\eta_b = (2.47 \pm 0.01)$ mPas,[17] and is thus of importance for interface-related phenomena and systematic model up-scaling. The influence of thermostats on the sampling of viscosities is interpreted in the phenomenological molecular relaxation picture described above.

2. METHODS

2.1. Green−Kubo Formulae and Pressure Tensors. In this work, shear viscosity and bulk viscosity were sampled with MD simulation and the Green−Kubo formalism. As derived originally by Mori,[18,19] both viscosities are determined in linear response theory by the total magnitude of the autocorrelation $C_{s,b}$ of the equilibrium fluctuations of pressure tensor components. Evaluations of shear and bulk viscosities $\eta_{s,b}$ are given by the infinite time limit of their respective cumulative integrals $\eta_{s,b}(t)$

$$C_s(\tau) = \langle \mathcal{P}_{\alpha,\beta}(\tau)\mathcal{P}_{\alpha,\beta}(0)\rangle_{\alpha\neq\beta} \tag{1}$$

$$C_b(\tau) = \langle (p(\tau) - \overline{p})(p(0) - \overline{p})\rangle \tag{2}$$

$$\eta_{s,b}(t) = \frac{V}{k_B T}\int_0^t \mathrm{d}\tau C_{s,b}(\tau) \tag{3}$$

where V is the volume, k_B is the Boltzmann constant, T is the temperature, and t is the integration time. $\eta_{s,b}(t)$ are called cumulative integrals of the autocorrelation functions $C_{s,b}$. $\mathcal{P}_{\alpha,\beta}$ is an off-diagonal element of the pressure tensor, $p(t) = \frac{1}{3}Tr(\mathcal{P})$, $\overline{p}$ is the mean pressure, and $\langle\cdots\rangle$ is the ensemble average over time origins. To improve statistics, an average over the three independent terms xy, xz, and yz can be drawn for the shear viscosity. Similarly, for the bulk viscosity nine terms can be averaged, three diagonal and six cross-terms,[20] which is mathematically equivalent to the direct use of the scalar pressure $p(t)$. In linear response theory, bulk and shear viscosities $\eta_{s,b}$ are evaluated in the limit of infinite time of their respective cumulative integrals. However, in practice, viscosities are estimated from a plateau at finite time reached by the cumulative integrated correlation functions, since long-time tail and noise accumulation lead to strong fluctuations[21] in the limit $t \to \infty$. In this work, the viscosity values were assessed at correlation times shortly after the first plateau was reached.

In the NVE ensemble, two expressions for the pressure tensor[22] entering the Green−Kubo formulae are commonly used. For a system of N molecules consisting of n atoms each and simulated in the NVE ensemble, the atom-based pressure tensor can be written as

$$\mathcal{P}_a^{NVE} = \frac{1}{V}\sum_{\mu=1}^{N}\sum_{i=1}^{n_\mu}\left[\frac{\mathbf{p}_{\mu i}\otimes\mathbf{p}_{\mu i}}{m_{\mu i}} + (\mathbf{r}_{\mu i}\otimes\mathbf{F}_{\mu i})\right] \tag{4}$$

where $\mathbf{r}_{\mu i}$, $\mathbf{p}_{\mu i}$, $m_{\mu i}$, and $\mathbf{F}_{\mu i}$ are position, momentum, mass, and force of atom i that is part of molecule μ, respectively. $\otimes$ represents the tensor product. Alternatively, a pressure tensor can be defined in a molecule-based form, where position $\mathbf{r}_\mu$, momentum $\mathbf{P}_\mu$, mass M_μ, and force $\mathbf{F}_\mu$ relate to the center of mass of molecule μ

$$\mathcal{P}_m^{NVE} = \frac{1}{V}\sum_{\mu=1}^{N}\left[\frac{\mathbf{P}_\mu\otimes\mathbf{P}_\mu}{M_\mu} + (\mathbf{r}_\mu\otimes\mathbf{F}_\mu)\right] \tag{5}$$

If simulations are not carried out in the NVE ensemble, but in the grand canonical (μVT) or NVT ensemble, each pressure term of the bulk autocorrelation function eq 2 has to be corrected by[23,24]

$$\left(\frac{\partial p}{\partial N}\right)_V (N - \overline{N}) + \left(\frac{\partial p}{\partial E}\right)_V (E - \overline{E}) \tag{6}$$

https://doi.org/10.1021/acs.jpcb.2c06035
J. Phys. Chem. B 2022, 126, 10172−10184

where N and E are the number of molecules and the Hamiltonian of the system, respectively, while $\overline{N}$ and $\overline{E}$ denote their time averages. The first term of eq 6 vanishes for all ensembles with a constant number of molecules, and the second term becomes zero for the NVE ensemble so that eq 4 or 5 is recovered, respectively.

In the NVT ensemble, only the second term of eq 6 is relevant since the number of molecules is constant

$$\mathcal{P}_{\mathrm{a,m}} = \mathcal{P}_{\mathrm{a,m}}^{\mathrm{NVE}} - \boldsymbol{I}\left(\frac{\partial p}{\partial E}\right)_{\mathrm{V}}(E - \overline{E}) \tag{7}$$

The thermodynamic relation

$$\left(\frac{\partial p}{\partial E}\right)_{\mathrm{V}} = \left(\frac{\partial p}{\partial T}\right)_{\mathrm{V}}\left(\frac{\partial T}{\partial E}\right)_{\mathrm{V}} = \frac{\gamma'}{C_{\mathrm{V}}} \tag{8}$$

with the thermal pressure coefficient γ' and the isochoric heat capacity C_{V} is introduced in eq 7. A knowledge of γ' and C_{V} allows for the application of the correction term in a post-processing step of the data sampled in the NVT ensemble. Table S3 in the Supporting Information summarizes the values obtained for the two water models considered. Heat capacity and thermal pressure coefficient values for TIP3P and TIP4P/2005 were sampled from standard fluctuation formulae,[25] employing the ms2 simulation package. The expression in eq 7 for the pressure tensor was taken into account when bulk viscosity data from thermostatted NVT samplings are reported, if not stated otherwise.

All pressure tensors, eqs 4, 5, and 7, allow naturally for a split in a kinetic and a virial part

$$\mathcal{P}_{\mathrm{a,m}} = \mathcal{P}_{\mathrm{K}} + \mathcal{P}_{\mathrm{V}} \tag{9}$$

in both NVE and NVT ensembles. The correction term in the NVT ensemble is included in the virial part. In any case, the split of the pressure tensor leads to three contributions to the autocorrelation functions

$$C_{\mathrm{b}}(\tau) = C_{\mathrm{K}}(\tau) + 2C_{\mathrm{KV}}(\tau) + C_{\mathrm{V}}(\tau) \tag{10}$$

when taking the traces of the pressure, kinetic and virial tensor into account, respectively. Here, the mean values of the kinetic and the virial part are subtracted from their respective dynamical counterparts. A similar splitting applies to the cumulative integrals, leading to three contributions to viscosity estimates according to eq 3.

The influence of the pressure tensor definitions, eqs 4 and 5, was tested in simulations in the NVE ensemble and found to be equivalent for the cumulative integral of the autocorrelation function; cf. Figure 1. These simulation results are consistent with the theoretical derivations in ref 26, where it had been shown that the difference of the infinite time integrals between atomic and molecular pressure autocorrelation functions vanish. The origin of this difference is related to the fact that the molecular definition of the virial is not necessarily symmetric; see again ref 26.

The center of mass pressure tensor leads to autocorrelation functions with much more pronounced short-time features than the atom-based pressure tensor. This finding implies that higher sampling rates are necessary when the center of mass pressure tensor is used.

It is worth mentioning that the estimation of macroscopic transport coefficients via autocorrelation functions is in general highly sensitive to the algorithm used.[27] Biased and unbiased estimators are commonly employed to analyze signals $s(i)$, i = 1, 2, ⋯, M in general. Using the standard unbiased mean value estimator $\overline{s} = 1/M \sum_i s(i)$, the biased estimator of the signal's autocorrelation function

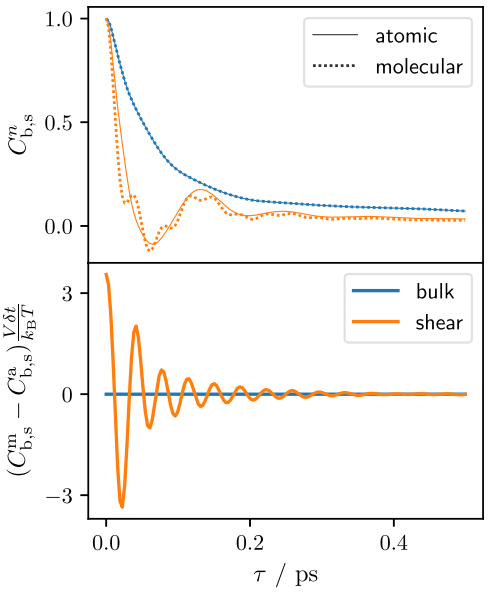

Figure 1. (Top) Normalized autocorrelation function $C^{\mathrm{n}}_{\mathrm{b,s}}$ of the trace and off-diagonal elements of the pressure tensor based on molecular (dashed line) and atomic (solid line) definitions, respectively. Signal taken from an NVE simulation of TIP4P/2005 water after equilibration at 300 K and 1 bar. (Bottom) Differences between both definitions of the pressure tensor. The integral of this damped sinusodal-like function is close to zero, which allows us to use both definitions for viscosity estimations.

$$C^{\mathrm{b}}(\tau) = \sum_{i=1}^{M-\tau} \frac{(s(i) - \overline{s})(s(i+\tau) - \overline{s})}{M} \tag{11}$$

has the advantage over the unbiased estimator

$$C^{\mathrm{u}}(\tau) = \sum_{i=1}^{M-\tau} \frac{(s(i) - \overline{s})(s(i+\tau) - \overline{s})}{M - \tau} \tag{12}$$

that the variance of the estimation is smaller.[28] Thus, if the goal is to estimate an autocorrelation function as close as possible to the true one using a given finite amount of samples, the biased estimator should be used. However, this approach cannot be employed here, since the integral of the autocorrelation function, up to the finite sampling time obtained by the biased estimator is necessarily zero; see ref 27 for a discrete proof. Viscosity data obtained from eq 2 and integrated up to the sampling time would be zero by construction, irrespective of the underlying pressure signal. Therefore, the unbiased estimator of the autocorrelation function was used in this work.

The evaluation of the autocorrelation functions was implemented as a post-processing step using fast Fourier transformation, followed by a subsequent Simpson integration to estimate the cumulative integrals from eqs 1 and 2 for each sampled trajectory.

2.2. Rotational Correlation Time and Hydrogen-Bond Lifetime. To characterize the collective dynamic properties of water, the rotational correlation time and the hydrogen-bond lifetime were investigated as well. Both properties are intrinsically connected to the bulk viscosity since their relaxation, characterized by the lifetime, following external

https://doi.org/10.1021/acs.jpcb.2c06035
J. Phys. Chem. B 2022, 126, 10172−10184

interventions has an influence on the bulk viscosity as discussed in the Section 1.

The rotational correlation time around a normalized water OH bond direction $\boldsymbol{e}^{\mathrm{OH}}$ is defined as

$$\tau_{\mathrm{rot}} = \int_0^\infty \langle P_l(\boldsymbol{e}^{\mathrm{OH}}(t)\cdot\boldsymbol{e}^{\mathrm{OH}}(0))\rangle dt \tag{13}$$

with $P_{l=2}$ the second-order Legendre polynomial, decaying to zero in the long time limit.

Following the integration scheme of refs 7, 29, the area is estimated from $t = 0$ to 5 ps by direct integration and from 5 ps $\leq t \leq$ 20 ps by integrating an exponential fit of the form $A_0 \exp(-t/\tau)$. Three independent simulations over 500 ps were conducted for each thermostat and damping pair, with a time resolution of 10 fs. From each simulation, three different molecules were used for averaging.

The continuous hydrogen-bond time correlation was sampled according to

$$S(\tau) = \langle h_{i,j}(t)H_{i,j}(t+\tau)\rangle / \langle h_{i,j}^2\rangle \tag{14}$$

where $h_{i,j}(t) = 1$, if a bond exists between atoms i and j at time t and zero otherwise. $H_{i,j}(t+\tau) = 1$, if the same bond exists for the full time range from t to $t+\tau$ and zero otherwise.[30] The average was taken over any hydrogen bond i, j which exists at a given time in the observed trajectory. In this work, the GROMACS hbond utility was used to obtain the hydrogen-bond existence map. A hydrogen bond was characterized geometrically: the distance between donor (oxygen bound to hydrogen) and acceptor atoms (oxygen of another molecule) has to be lower than 3.5 Å and the angle between hydrogen atom, donor atom, and acceptor atom has to be lower than 30°.[31,32]

$S(\tau)$ decays to zero for large times since diffusion in liquid water ensures that hydrogen bonds break at some point. The hydrogen-bond lifetime is then defined as the integral

$$\tau_{\mathrm{hb}} = \int_0^\infty S(t)\mathrm{d}t \tag{15}$$

For each thermostat and damping pair, three independent simulations were conducted, of which 30 ps were used for sampling. The hydrogen-bond map, as sampled by the GROMACS hbond utility, was further processed with the help of the python package MDAnalysis[33,34] to estimate the lifetime via eq 15.

2.3. Overview of MD Packages and Thermostats Used. As usual in molecular dynamics and motivated by the equipartition theorem, the instantaneous temperature is defined as a measure for the fluctuating kinetic energy

$$T(t) = \frac{2}{N_{\mathrm{DOF}}k_{\mathrm{B}}}E_{\mathrm{kin}}(t) \tag{16}$$

This definition is adapted by the MD packages and thermostats used in this work. Each water molecule contributes six degrees of freedom since they are treated as rigid bodies by the force fields used.

The MD packages NAMD[35] (version 2.13), GROMACS[31,32,36−41] (version 2021.2), and ms2[42,43] (version 4.0) were used in this work. Some of the basic differences between these packages are the handling of the long-range electrostatic interactions and the numerical integration schemes to solve Newton's equations of motion. While NAMD and GROMACS use integrators based on extensions of the Verlet algorithm, ms2 uses a Gear fifth-order integration scheme. Long-range electrostatics is handled in NAMD by the particle-mesh Ewald method, ms2 uses the reaction field method,[25] while in GROMACS, both methods are implemented.

Most simulations were performed in the NVT ensemble to study the influence of various thermostats on the resulting shear and bulk viscosity values. Table 1 lists the considered thermostats. Two velocity-randomizing approaches were tested, i.e., Langevin and Andersen-massive, together with four velocity scaling thermostats, i.e., Nosé−Hoover, Berendsen, velocity rescaling, and stochastic rescaling.

Table 1. Thermostats Used in This Work

type	thermostat	MD package
randomizing	Langevin	NAMD, GROMACS[32,44]
	Andersen-massive	GROMACS[3,32]
scaling	Nosé-Hoover	GROMACS[4,32]
	Berendsen	GROMACS[5,32]
	stochastic rescaling	NAMD, GROMACS[6,32,44,45]
	velocity rescaling	NAMD, ms2[43,44]

A brief summary of the behavior of the thermostats is given here, a detailed introduction can be found in ref 7. In general, to maintain a constant temperature, the system is coupled to a fictitious heat bath at the target temperature T_0, either by changing molecule velocities or Newton's equation of motion. As a result, dynamics is altered compared to NVE simulation results.

The common descriptor to compare thermostat influence will be the inverse coupling strength or damping γ in units of ps^{-1}, even though this property does not have the same meaning for all thermostats. The microcanonical limit is reached for $\gamma \to 0$ with looser binding of the heat bath to the system, while tighter control of the temperature requires a larger γ.

The Andersen-massive thermostat randomizes the velocities of all molecules at time intervals of γ^{-1} taken from a Maxwell−Boltzmann distribution. This has the advantage that the equation of motion does not change.

A widely used thermostat in biomolecular simulations is the Langevin thermostat. The Langevin equation of motion adds a friction term with a damping constant γ and a noise term depending on γ and the target temperature, which remove or add energy, respectively. The interplay between friction and randomness respects the fluctuation-dissipation theorem.[46] In this study, the same value of γ was used for all molecules, whereas it is possible to apply different values to individual or groups of molecules.[7,32,44]

Instead of randomizing, the following thermostats scale the velocities to maintain the target temperature. The Berendsen thermostat is based on an exponential decay of temperature $\mathrm{d}T(t)/\mathrm{d}t = \tau^{-1}[T_0 - T(t)]$ toward its target value, where the time constant is $\tau = 2C_v/(N_{\mathrm{DOF}}k_{\mathrm{B}}\gamma)$, the number of degrees of freedom N_{DOF}, and the isochoric heat capacity C_v. The disadvantage of this method is that the velocity distribution is noncanonical because kinetic energies close to T_0 are favored. This issue is addressed in the thermostat proposed by Bussi et al.,[6] which is referred to as stochastic rescaling.[7] It modifies the Berendsen kinetic energy equation by introducing an additional stochastic term, which restores the kinetic energy fluctuations as expected in the canonical ensemble.

https://doi.org/10.1021/acs.jpcb.2c06035
J. Phys. Chem. B 2022, 126, 10172−10184

Table 2. Overview of Systems Simulated in This Study at T = 300 K, p = 1 bar

	system 1	system 2	system 3
water model	TIPS3P	TIP4P/2005	TIP4P/2005
atoms/molecules	9309/3103	3728/932	-/1372
volume (nm^3)	4.78 × 4.37 × 4.377	3.01 × 3.01 × 3.01	3.45 × 3.45 × 3.45

The Nosé−Hoover thermostat scales the velocities by means of the momentum $p_\xi = Q\mathrm{d}\xi/\mathrm{d}t$ of an extended heat bath ξ that is coupled to each molecule i. The temperature of the system converges to T_0 in an oscillatory manner. The altered equations of motion for $\mathbf{r}_i$ and ξ are given by

$$\frac{\mathrm{d}^2\mathbf{r}_i}{\mathrm{d}t^2} = \frac{\mathbf{F}_i(\mathbf{r}_i)}{m_i} - \frac{p_\xi}{Q}\frac{\mathrm{d}\mathbf{r}_i}{\mathrm{d}t}$$
$$\frac{\mathrm{d}^2\xi}{\mathrm{d}t^2} = \frac{T - T_0}{Q} \tag{17}$$

where Q is the inertia of the heat bath defined in GROMACS as $Q = T_0/(4\pi^2\gamma^2)$. Phase-space sampling can be enhanced via serial coupling to multiple heat baths, the so-called Nosé−Hoover chains.[47] However, the present study is restricted to the original Nosé−Hoover thermostat.

NAMD offers the possibility to apply plain velocity rescaling at γ^{-1} intervals by multiplying each molecule's velocity with $\sqrt{(T_0/T)}$. Using the time step of the integrator as rescaling interval, the standard velocity rescaling algorithm is recovered in NAMD as implemented for the NVT ensemble in ms2.

2.4. Simulation Details. Two well-known rigid water models, i.e., TIPS3P[48] and TIP4P/2005,[49] were considered in this work. The TIPS3P model differentiates from the original TIP3P[50] model through additional Lennard-Jones sites placed on the hydrogen atom positions. The four-site TIP4P/2005[49] model was employed in its original form taken from the website of the Vega group.[49,51]

The simulation volumes were prepared and equilibrated under the conditions given in Table 2. Throughout, periodic boundary conditions were chosen. For systems 1 and 2, a switching distance of 1.0 nm and a cutoff radius of 1.2 nm were applied for the Lennard-Jones interactions. Long-range electrostatic interactions were handled with the particle-mesh Ewald (PME) method with a cutoff radius of 1.2 nm.[32,44] A time step of 2 fs was chosen for the NVT simulations and 0.8/1 fs for NVE simulations to enhance energy conservation.

Systems 1 and 2 were constructed by randomly placing water molecules into the volume. Then, a potential energy minimization was carried out with a steepest gradient method. Subsequently, the volume was relaxed in the NpT ensemble using a Langevin thermostat and Langevin piston barostat[52,53] for 1 ns. An NVT simulation was then performed for another 1 ns using the volume output from the last NpT frame. Note that system 1 was slightly anisotropic. Throughout test simulations with cubic and slightly noncubic boxes, no significant differences due to anisotropy were found in the sampled autocorrelations and cumulative integrals. For each combination of program, thermostat, and ensemble, 20 independent simulations over 6 ns were conducted. The values for the bulk and shear viscosities were obtained for each single simulation as outlined before. Average and standard deviation were obtained from 20 independent trajectories, and the latter is reported as statistical uncertainty. System 3 was simulated with the ms2 package[42,43] in a cubic volume with a cutoff radius of r_c = 1.55 nm. Newton's equation of motion was solved with a fifth-order Gear predictor-corrector integrator with a time step of 0.877 fs. Lennard-Jones long-range interactions were considered analytically. Long-range electrostatic interactions were approximated by the reaction field technique with conducting boundary conditions ($\epsilon_{RF} = \infty$).

Simulations using ms2 (system 3) were performed in two steps, a first simulation over 10^6 time steps in the NpT ensemble was carried out to calculate the density and the Hamiltonian. In a second step, these values were used in the simulations in the NVT and NVE ensembles, which were additionally equilibrated over 5×10^5 time steps, followed by five production runs of 2.5×10^7 time steps.

2.5. Validation. To assess the equilibration procedure on the basis of literature results, a cross-validation with respect to the self-diffusion coefficient of TIPS3P water was conducted in the NVE ensemble with a time step of 2 fs, as well as in the NVT ensemble at 300 K and 1 bar using a Langevin thermostat with varying coupling strengths. The self-diffusion coefficient was sampled with the Einstein formula resting on the mean-squared displacement (MSD)[25]

$$D = \lim_{t\to\infty} \frac{1}{6Nt} \sum_{i=1}^{N} \langle r_i(t + t_0) - r_i(t_0)^2 \rangle \tag{18}$$

Therein, $\langle\rangle$ is an ensemble average over five molecules and a time average over all available time origins t_0. Twenty independent simulations with a time step of 2 fs over 6 ns each were conducted. The snapshots used have a time difference between the frames of Δt = 1 ps. MSD data were averaged and the self-diffusion coefficient D was then determined from a linear fit in the range 0 ps ≤ t ≤ 2000 ps to avoid noisy data due to insufficient sampling with a large lag time. The results reproduce the findings from ref 7, if the Yeh and Hummer[54] finite size correction is taken into account;[55] cf. Figure 2. Self-diffusion coefficients calculated without the finite size correction are listed in Table S4 in the Supporting Information, and the values of finite size corrections are on the order of 0.6 × 10^{-5} cm^2 s^{-1}. These results indicate that the employed systems were properly equilibrated and that the simulation protocols were implemented correctly. Subse-

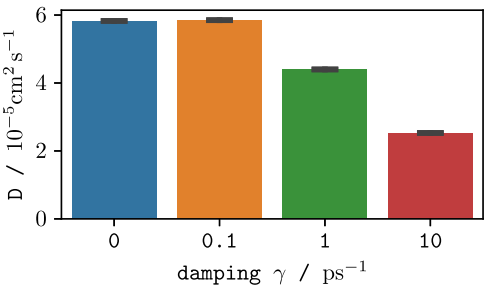

Figure 2. Self-diffusion coefficient of the TIPS3P model at 300 K and 1 bar sampled with NAMD in the NVT ensemble with the Langevin thermostat for different coupling strength γ including NVE result (blue bar) γ = 0 ps^{-1}.

https://doi.org/10.1021/acs.jpcb.2c06035
J. Phys. Chem. B 2022, 126, 10172−10184

Table 3. Viscosity Values for the Studied Water Models at 1 bar from the Literature[a]

ensemble	water model	long-range	T (K)	η_b(mPa·s)	η_s(mPa·s)	year	refs
NVE	TIP4P/2005	ES	298	2.065 ± 0.106	0.807 ± 0.017	2012	56
NVE	TIP4P/2005	ES	303	1.981 ± 0.092	0.753 ± 0.015	2012	56
NVE	TIP4P/2005	PME	298		0.855	2010	57
NVT	TIP4P/2005	RF	298.15		0.89 ± 0.09	2011	58
NVT	TIP4P/2005	ES	300		0.83 ± 0.05	2012	59
NVT	TIP4P/2005	ES	300		0.826 ± 0.1	2019	60
NVT (NEMD)	TIP4P/2005	PME	300.2		0.31	2006	61
NVE	TIP3P	PPPM	298		0.31	1996	62
NVE	TIP3P	PME	300		0.306 ± 0.04	2013	7
NVT	TIP3P	PME	298		0.321	2010	57
NVT	TIP3P	PME	298		0.308 ± 0.1	2004	54
NVT (NEMD)	TIP3P	PPPM	300		0.318	2012	63
NVT	TIP3P	ES	298.15		0.315	2019	64
NVT	TIP3P	PME	298.15		0.329 ± 0.001	2010	65
NVT (NEMD)	TIP3P	PME	300		0.325	2010	66
NVT	TIP3P	PME	300		0.3 ± 0.04	2014	67
	experimental		298	2.47 ± 0.01	0.888 ± 0.01	2011	17

[a]Treatment of the long-range electrostatic interactions: Ewald summation (ES), particle-mesh Ewald (PME), particle−particle particle-mesh (PPPM), and reaction field (RF).

quently, these equilibration and simulation protocols were employed throughout for both water models to investigate the viscosities. The influence of the damping value γ on the self-diffusion coefficient is clearly demonstrated in Figure 2 so that it is expected that the viscosity values sampled with the Green−Kubo formalism will also be influenced by the thermostat setup.

3. RESULTS AND DISCUSSION

Transport properties can be obtained from molecular observables employing linear response theory and the Green−Kubo formalism. Thus, at a given thermodynamic state point, the force field solely determines the sampled viscosities, regardless of the ensemble used. However, it turns out that the numerical evaluation of the bulk and shear viscosities is challenging.

Literature results, summarized in Table 3, reveal that only few data are available for the bulk viscosity of water sampled with molecular dynamics in the NVE and NVT ensemble; this gap is closed in this work.

Throughout, the simulation volumes were equilibrated for TIPS3P or TIP4P/2005 water following the procedure described above. In a first step, pressure tensor autocorrelation functions and hence the bulk and shear viscosities were sampled in the NVE ensemble. Finally, a detailed analysis of the role of thermostats in the NVT ensemble is presented, which is the core part of this work. In particular, the relevance of the correction term in eq 7 is investigated as a function of the thermostat coupling strength γ.

Results presented below, which were obtained using GROMACS or ms2, are indicated by a prefix gmx or ms2, respectively. If no prefix is given then the corresponding result was obtained using NAMD.

3.1. Sampling Viscosities in the Microcanonical Ensemble. MD simulations in the NVE ensemble were performed for TIP4P/2005 water with ms2, NAMD, and GROMACS. The resulting long-time behavior of the cumulative integrals of the pressure tensor autocorrelation functions $\eta_s(t)$ and $\eta_b(t)$, cf. eqs 1 and 2, is presented in Figure 3. The corresponding normalized autocorrelation functions are shown in Figures S8 and S9 in the Supporting Information.

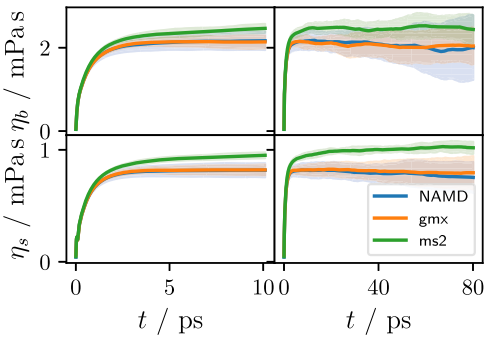

Figure 3. Bulk (top) and shear (bottom) viscosities of TIP4P/2005 water sampled with different packages in the NVE ensemble at 300 K and 1 bar at two different timescales.

Integrated pressure autocorrelation functions sampled with GROMACS and NAMD, both using PME, exhibit the same short-time behavior for the bulk and shear viscosities. On the other hand, autocorrelation functions sampled with ms2, using the reaction field method, exhibit a somewhat slower convergence of the cumulative integrals and lead to slightly higher viscosity values at the first plateau; cf. Figure 3.

To evaluate the influence of the long-range nonbonded method on the sampled viscosity data, simulations with GROMACS were also carried out using the reaction field method. As can be seen in Figure 4, an increase of both sampled viscosities was observed when the reaction field is used, which is consistent with the results obtained with ms2. This demonstrates that the methods for long-range electrostatics have a non-negligible influence on sampled shear and bulk viscosities, which has also been observed in the literature for diffusion coefficients and rotational correlations.[29]

It should be noted that the slower short-time convergence of the cumulative integrals sampled with ms2 was not reproduced by GROMACS; cf. Figure 4. This difference could originate

https://doi.org/10.1021/acs.jpcb.2c06035
J. Phys. Chem. B 2022, 126, 10172−10184

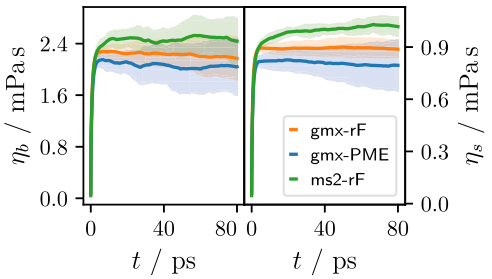

Figure 4. Bulk and shear viscosities of TIP4P/2005 water sampled in the NVE ensemble at 300 K and 1 bar employing either reaction field (rF) or particle-mesh Ewald (PME) treatment of long-range electrostatics.

from different numerical integration schemes, as GROMACS employs a Verlet integrator and ms2 rests on a Gear integrator.

A similar cross-validation between simulation results for the shear and bulk viscosities sampled with NAMD and GROMACS for TIPS3P water is shown in Figure 5. Consistent with the observations for TIP4P/2005 water, both simulation tools yield equivalent results. Moreover, they are able to reproduce other literature values; cf. Table 3.

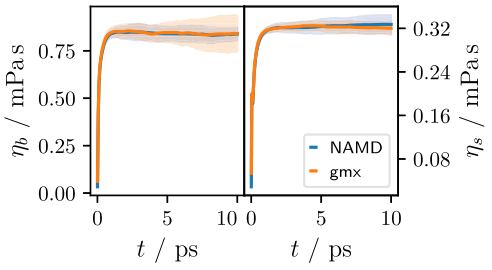

Figure 5. Bulk and shear viscosities of TIPS3P water sampled in the NVE ensemble at 300 K and 1 bar with GROMACS (orange) and NAMD (blue).

All conducted NVE runs show stable potential and kinetic energy values at the desired temperature. Therefore, NVE results for bulk and shear viscosities are used as a reference for comparison with the results obtained from NVT ensemble simulations.

The variance of the instantaneous temperature, eq 16, is denoted by δT^{NVE} and usually identified with its mean fluctuations since the variance is sampled from a trajectory. In the NVE ensemble,[68] δT^{NVE} is given by

$$\delta T^{\mathrm{NVE}} = \frac{\sqrt{2}\,T_0}{\sqrt{N_{\mathrm{DOF}}}}\sqrt{1 - \frac{6k_{\mathrm{B}}}{2c_{\mathrm{V}}}} \tag{19}$$

where c_{V} is the isochoric heat capacity per molecule. Table 4 summarizes the results obtained from the present simulation runs.

According to eq 19, the expected value for δT^{NVE} is 2.505 K, consistent with the results in Table 4.

Table 4. Mean Temperature T and Mean Fluctuations δT of 3103 Water Molecules in the NVE Ensemble

package	long range	T(K)	δT (K)
NAMD	PME	300.4(7)	2.49(2)
GROMACS	PME	300.7(6)	2.50(3)

Temperature fluctuations (variances) in the NVE ensemble are different from the fluctuations (variances) expected in the NVT ensemble given by[69]

$$\delta T^{\mathrm{NVT}} = \frac{\sqrt{2}\,T_0}{\sqrt{N_{\mathrm{DOF}}}} \tag{20}$$

at temperature T_0. Comparing eqs 19 and 20 reveals that temperature fluctuations are significantly lower in the NVE ensemble than in the NVT ensemble, eq 20 at 300 K and for 3103 water molecules yields 3 K. In the NVT simulations below, the instantaneous temperature fluctuations were used as one sampling result indicating equilibrium.

3.2. Sampling Viscosities in the Canonical Ensemble.

3.2.1. TIPS3P. Figure 6 shows the bulk viscosity cumulative integrals for the TIPS3P water model. Simulations employing the Berendsen and Nosé–Hoover thermostat were performed with GROMACS, all other thermostats were executed with NAMD. The results highlight the importance of taking the correction term, eq 6, into account while sampling the bulk viscosity.

Without the correction term, Figure 6, and in particular for low damping used in Andersen-massive, Langevin, stochastic rescaling, and Nosé–Hoover thermostats, spurious unphysical cumulative bulk viscosity integrals were obtained. Overall, for all thermostats and damping values, this non-negligible correction reduces the sampled bulk viscosity. Therefore, ensemble-corrected values for η_{b} are reported for all NVT simulations.

The role of the correction term, eq 6, was further investigated for the Langevin thermostat. Note that the simulations performed in this work with it reproduce the shear viscosity results from ref 7 for different values of the damping parameter γ. The Langevin thermostat, for all finite damping values, is known to be ergodic[70] with respect to the canonical distribution function. Since the kinetic energy fluctuations in the NVE ensemble are lower than in the NVT ensemble, the thermostat necessarily restores the canonical fluctuations as exemplified in Figure S2 in the Supporting Information. But for weaker damping, it takes longer for the temperature fluctuations to approach the canonical distribution; see Figure S1 in the Supporting Information. The role of the correction term in the low-γ limit is visible in the enhanced autocorrelation of the instantaneous kinetic pressure and its effect on the bulk viscosity cumulative integrals is revealed in Figure 7. These autocorrelations are calculated analogous to eq 1 for the kinetic and virial part, and the cross-term according to eqs 9 and 10. While the virial–virial cumulative integral is only weakly affected for low γ by the Langevin thermostat, kinetic-kinetic and kinetic–virial cumulative integrals show a clear dependence on the damping parameter. In general, the ensemble correction led to a compensation of the spurious long-ranged kinetic autocorrelation by a negative contribution of the kinetic–virial part to the bulk viscosity cumulative integral, and this compensation in the low-γ limit is almost complete.

Figure 8 summarizes the results for bulk and shear viscosities sampled in this work. Velocity-randomizing thermostat approaches, like Langevin and Andersen-massive thermostats, drastically influence the sampling results for shear and bulk viscosities for damping values of $\gamma > 1$ ps^{-1}. For the shear viscosity of the TIPS3P water model, this behavior has already been observed in the literature.[7] In this work, a similar result

https://doi.org/10.1021/acs.jpcb.2c06035
J. Phys. Chem. B 2022, 126, 10172–10184

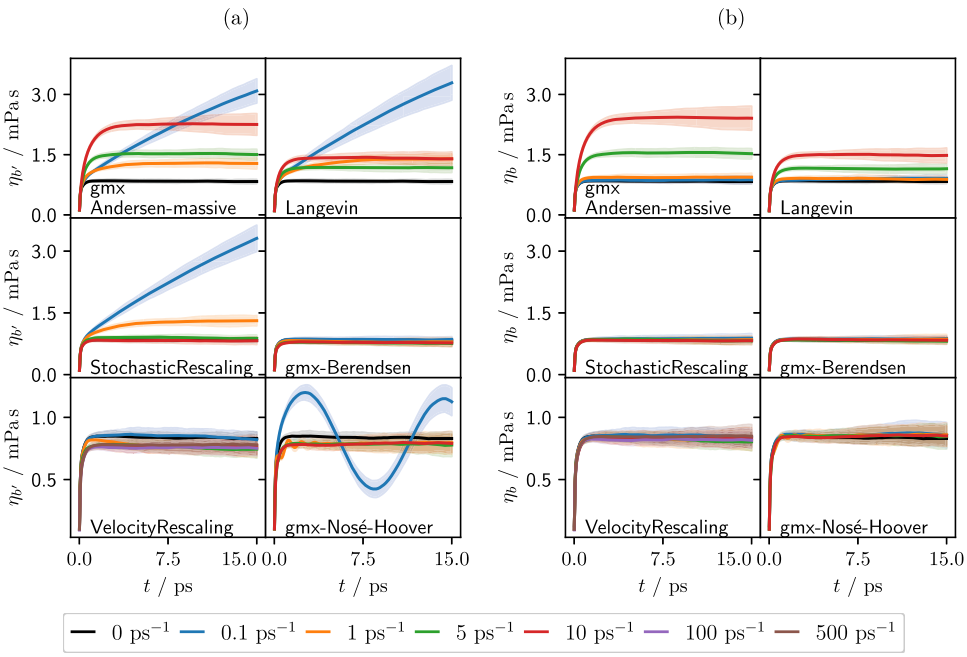

Figure 6. Cumulative bulk viscosity integrals in the NVT ensemble, (a) $\eta_{b'}$ without correction term and (b) η_b with correction term, for the TIPS3P water with various thermostats and coupling strengths including NVE results as black lines (0 ps^{-1}).

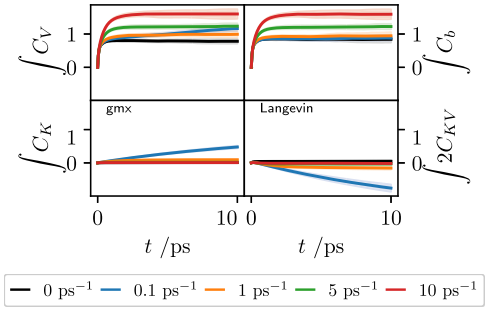

Figure 7. Summands of the bulk viscosity cumulative integrals (in units of mPa·s) for TIPS3P water at 300 K and 1 bar with the Langevin thermostat with GROMACS for varying damping values γ including NVE results (black lines).

was found for the bulk viscosity. In the limit of low damping, the influence of thermostats on sampled viscosities is almost negligible.

Velocity rescaling thermostats, like stochastic rescaling, Berendsen, velocity rescaling, and Nosé−Hoover, introduce a more gentle effect on the viscosity data. For stochastic rescaling and Nosé−Hoover thermostats at low damping, the effect of the correction term, eq 6, is clearly visible for the bulk viscosity, Figure 6. In particular for stochastic rescaling, this has to be expected since it was shown that for low γ stochastic rescaling and Langevin thermostats influence collective variables in an equivalent manner.[71] The influence of velocity rescaling thermostats is seen to be negligible for a wide range of damping values, see Figure 8, and is in general within statistical uncertainties. Sampled numerical values for bulk and shear viscosities for TIPS3P water employing different thermostats and damping values are summarized in Table S1, and the corresponding autocorrelation functions are depicted in Figures S4 and S5 in the Supporting Information.

To further analyze the role of thermostats, including their coupling strength γ, collective dynamic variables were studied. In Figure 8b, the rotational correlation time and the hydrogen-bond lifetime are shown. Data were sampled from three

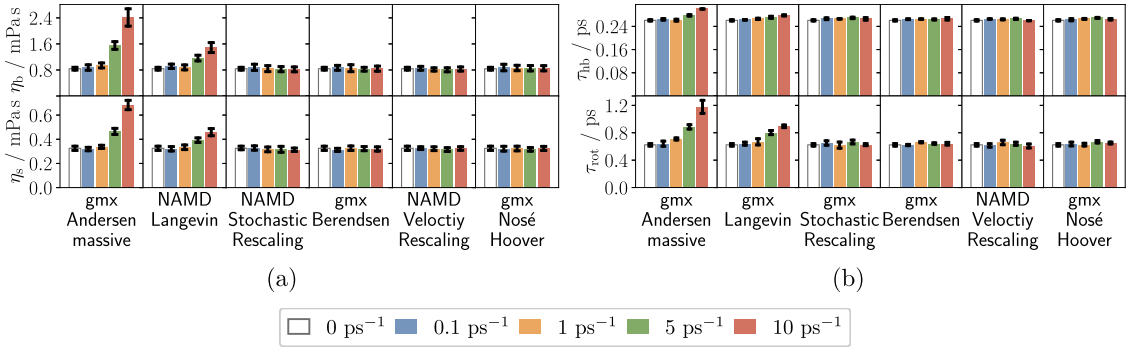

Figure 8. (a) (Top) Bulk and (bottom) shear viscosity calculated for TIPS3P water with various thermostats and damping values γ. (b) Hydrogen-bond lifetime τ_{hb} and rotational correlation time τ_{rot} of TIPS3P water for six different thermostats including NVE results (white bars). All data were simulated at 300 K and 1 bar.

https://doi.org/10.1021/acs.jpcb.2c06035
J. Phys. Chem. B 2022, 126, 10172−10184

independent 500 ps simulations using three molecules for averaging. In NVE simulations, a hydrogen-bond lifetime of 0.26 ps was found, which compares well to the literature value[72] of 0.29 ps reported for bulk water with sampling time separations of 16 fs. In the present work, a sampling time separation of 10 fs was used, which explains the difference: checking the bonds less frequently increases the apparent lifetime since bond breaking and reformation between two frames are counted as unbroken.

It was found that only the velocity-randomizing thermostats (Andersen-massive and Langevin) with strong coupling increase the lifetime of hydrogen bonds and the rotational correlation time. In the limit of low γ, the NVE results are approached. In the medium-to-high-γ regime, the hydrogen-bond lifetime and the rotational correlation time are both prolonged, which can be interpreted as a slowdown of collective dynamics. A similar behavior was reported in the literature for rotations.[7] Thus, velocity-randomizing thermostats induce a stabilizing effect on collective variables, which leads to longer relaxation times upon small equilibrium disturbances. This prolongation induces a higher apparent bulk viscosity as discussed in the phenomenological model that was briefly introduced above and elaborated in detail in ref 9. This influence of velocity-randomizing thermostats is clearly visible in the sampled bulk viscosity data; cf. Figure 8. In the high-γ limit, Basconi and Shirts[7] already showed that collective dynamics, characterized by transport coefficients, is slowed down leading to prolonged correlations and thus to spuriously higher estimations of transport coefficients. In the present work, this slowdown is demonstrated for the sampling of the bulk viscosity in Figure 6.

Moreover, simulations with the Langevin thermostat were performed with GROMACS to assess differences between thermostat implementations. The results on cumulative integrals exhibit a fairly similar behavior over the studied damping range and mostly converge within statistical uncertainties to the same viscosity results; cf. Figure 9.

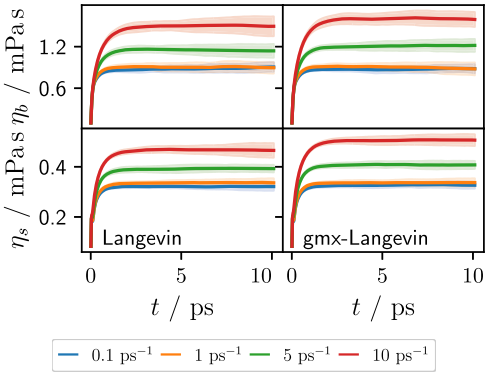

Figure 9. Bulk (top) and shear (bottom) viscosity cumulative integrals of TIPS3P water at 300 K and 1 bar using NAMD (left) and GROMACS (right) with the Langevin thermostat.

Furthermore, the same behavior of the sampled bulk viscosity with low damping parameter values was found for both implementations of the Langevin thermostat. The remaining small differences between the two implementations are attributed to different integration schemes. While NAMD is using a so-called BBK scheme,[35,73] GROMACS uses an impulse-like algorithm.[32,74] Thus, even different discretization schemes induce small differences in the thermostat-triggered relaxation processes and therefore may lead to small differences in the sampled bulk viscosity results. Nevertheless, the consistency achieved in this work using two simulation code packages is not self-evident; see the discussion in ref 75.

3.2.2. TIP4P/2005. NVT sampling results for bulk and shear viscosities for TIP4P/2005 water are summarized in Figure 10a and in Figure S7 in the Supporting Information, where the cumulative integrals are shown. Simulations employing Berendsen and Nosé−Hoover thermostats were performed with GROMACS, simulations employing all other thermostats were done with NAMD. The correction term, eq 6, was taken into account while sampling bulk viscosities. Viscosity values estimated from the cumulative integrals are compiled in Table S2, and the sampled autocorrelation functions are depicted in Figures S8 and S9 in the Supporting Information.

The role of the correction term, eq 6, was also investigated; cf. Figure S6 in the Supporting Information. Qualitatively, similar findings to the TIPS3P case discussed above were found, but they are quantitatively smaller. This is especially reflected in the value of the thermal pressure coefficient, which is much closer to the experimental value of water; cf. Table S3 in the Supporting Information. In particular for small damping values and for Langevin, Andersen-massive, stochastic rescaling, and Noise−Hoover thermostats, the ensemble correction was found to be important for a correct interpretation of the bulk viscosity cumulative integrals and hence for the sampled bulk viscosity.

NVT simulations employing velocity-randomizing thermostats yield drastically higher values of the bulk and shear viscosities for damping parameter values of about $\gamma > 1$ ps^{-1}, whereas NVE results are recovered for weak coupling, i.e., $\gamma \to 0$.

All NVT simulations performed with a velocity scaling thermostat were able to reproduce the shear and bulk viscosities sampled in the NVE ensemble within their statistical uncertainties.

In accordance with the results obtained in the NVE ensemble, cumulative integrals of the shear and bulk viscosities sampled with the ms2 tool converge slower than the ones sampled with NAMD when the velocity rescaling thermostat is used. This discrepancy could mainly be traced back to differences in the employed long-range electrostatics methods: NAMD uses PME, while ms2 uses the reaction field method. Velocity rescaling in each time step, i.e., with $\gamma = 500$ ps^{-1} for a time step of 2 fs, which is equivalent to ms2 velocity scaling, showed a good performance for all studied damping parameter values. Higher values of the bulk viscosity obtained with ms2 are again related to the different handling of long-range electrostatics.

Similar to the TIPS3P results, only the velocity-randomizing thermostats (i.e., Andersen-massive and Langevin) using high damping values increase the lifetime of hydrogen bonds and rotational correlation time by slowing down the dynamics of collective variables, which explains the higher bulk viscosity sampled in these cases, consistent with the phenomenological relaxation model.

A comparison of thermostat implementations was also performed for TIP4P/2005 water. Like in the TIPS3P simulations described above, NAMD and GROMACS yield comparable results when the Langevin thermostat is used to sample bulk and shear viscosities; cf. Figure 11. Small differences for higher damping values are still present, which can be attributed to different numerical schemes used in these

https://doi.org/10.1021/acs.jpcb.2c06035
J. Phys. Chem. B 2022, 126, 10172−10184

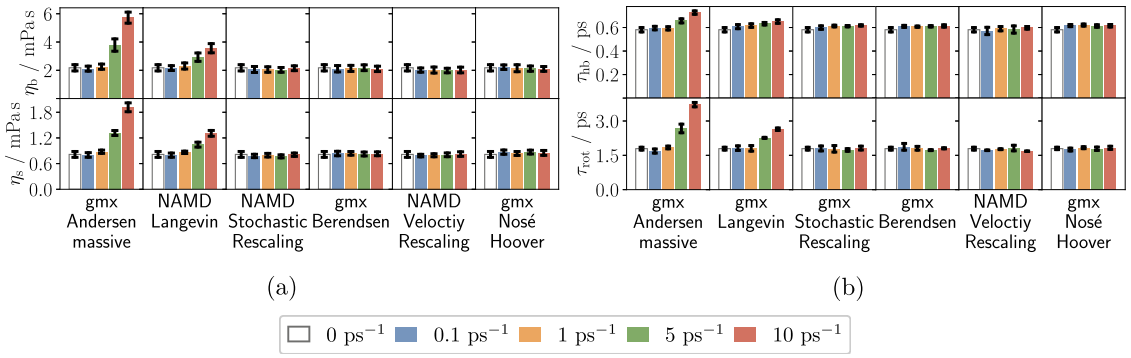

Figure 10. (a) (Top) Bulk and (bottom) shear viscosity calculated for TIP4P/2005 water with various thermostats and damping values γ. (b) Hydrogen-bond lifetime τ_{hb} and rotational correlation time τ_{rot} of TIP4P/2005 water for six different thermostats including NVE results (white bars). All data were simulated at 300 K and 1 bar.

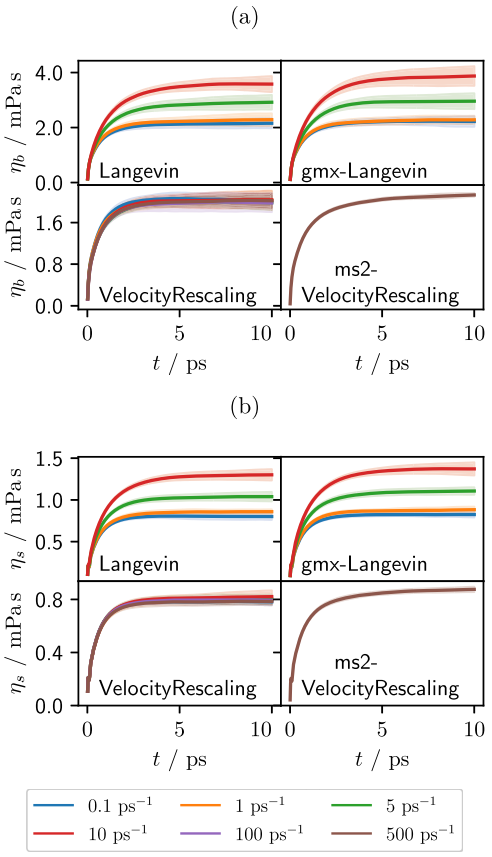

Figure 11. (a) Bulk and (b) shear viscosities of TIP4P/2005 water in the NVT ensemble at 300 K and 1 bar. Simulation results obtained with the Langevin thermostat with NAMD (left) and GROMACS, velocity rescaling with NAMD (left) and ms2.

packages. In accordance with the results obtained in the NVE ensemble, cumulative integrals of the shear and bulk viscosities sampled with ms2 converge slower than the ones sampled with NAMD using the velocity rescaling thermostat with a damping and time step leading to velocity rescaling in each time step. This discrepancy could mainly be traced back to differences in the employed long-range electrostatics treatment: NAMD uses PME while ms2 uses the reaction field method. Thus, the findings for the TIP4P/2005 water model are consistent with the TIPS3P water results.

In general, the influence of thermostats and corresponding damping values on sampled cumulative integrals and viscosities is qualitatively similar for TIPS3P and TIP4P/2005, but the TIP4P/2005 model shows a lower sensitivity of the sampled shear and bulk viscosities compared to TIPS3P results. Furthermore, as expected, the sampled bulk and shear viscosities for TIP4P/2005 water compare better with experimental data; cf. Table 3.

4. CONCLUSIONS

An investigation of the role of thermostats in sampling bulk and shear viscosities of liquid water with molecular dynamics was conducted. It turned out that the application of the Green−Kubo formalism, based on microscopic expressions for the pressure tensor, is not straightforward for water models in the NVT ensemble.

As a reference, simulations in the NVE ensemble with a mean temperature of 300 K were conducted, since the Green−Kubo formulae for the bulk and shear viscosities and their application in this ensemble are not under debate in the literature. The sampled viscosity values in the NVE ensemble were used as a reference for an assessment of different thermostat schemes. In agreement with literature results, mostly for the shear viscosity, it was found that the TIP4P/2005 model outperforms TIPS3P significantly.

In the NVE ensemble, a first challenge is posed by different definitions of the virial expression of the pressure tensor used for sampling the pressure autocorrelation function, and hence viscosities, using the Green−Kubo formalism. It was found that the molecular and atomic expressions lead to different autocorrelation functions for the off-diagonal pressure tensor elements with the somewhat surprising result that the molecular averaged definition leads to more features in the autocorrelation function. However, their influence on the shear viscosity is negligible since the difference is close to a damped sinusoidal function that does not contribute to the viscosity integrals, so both pressure tensors may be used. However, in the case of the studied water models, it was found that long-range electrostatic interaction treatments have an influence on the viscosity results beyond their statistical uncertainties.

Another challenge is the estimation of pressure autocorrelation functions from molecular dynamics time series. As discussed in Section 2, there are popular biased estimators, whose statistical properties are such that integrating autocorrelation functions up to the sampling time leads to useless results. This is a consequence of estimating the mean pressure and the autocorrelation functions simultaneously from

https://doi.org/10.1021/acs.jpcb.2c06035
J. Phys. Chem. B 2022, 126, 10172−10184

the same time series. Therefore, a standard unbiased estimator was used in this work and is recommended in general.

In the NVT ensemble, the correction according to eq 6 for the diagonal terms of the pressure tensor was shown to be important and was therefore taken into account throughout this paper. The influence of this correction was demonstrated to be highly dependent on the thermostat and the damping parameter, which reflects that thermostats are in general designed to sample time-independent observables in molecular dynamics and induce widely different effects into the dynamics of collective variables.

Velocity randomized thermostats (Andersen-massive, Langevin) were found to be inadequate for sampling pressure autocorrelation functions, and hence viscosities, for larger damping values. This can be interpreted as a slowdown of collective dynamic variables, already observed by other authors, which leads to slower relaxations. For the bulk viscosity, this relates directly to phenomenological entropy production terms in continuum-mechanic descriptions of the bulk viscosity. This slowdown of collective variables was demonstrated in this work for hydrogen-bond dynamics, and previous findings from the literature regarding the slowdown of rotations are confirmed. Both lead to higher bulk and shear viscosity estimations sampled in the canonical ensemble when randomizing thermostats with larger damping values are used.

Velocity rescaling thermostats (Berendsen, stochastic rescaling, Nosé–Hoover, velocity rescaling) were found to induce small effects on the sampled viscosities, although the relative importance of the pressure correction for the bulk viscosity is highest for stochastic rescaling and Nosé–Hoover thermostats. Nevertheless, the correction term is highly effective even at lower damping, leading to reliable viscosity estimates for all studied damping values. Thus, thermostats of this type should be used for viscosity sampling.

Three molecular dynamics simulation packages were used mainly for two reasons: first, not every thermostat is readily implemented in a single package, and second, to compare the viscosity results obtained from different simulation packages in the sense of cross-validation. In cases where a particular thermostat is implemented in multiple packages, only minor differences were found for the sampled viscosity data when the same numerical handling of long-range electrostatics was employed. Minor differences are attributed to different discretization schemes used to implement the same thermostat.

We recommend to take these conclusions into account in particular in systematic up-scaling procedures constructing or parameterizing models on higher scales, where the microscopic details are "integrated out" and represented as effective terms in dynamic equations, e.g., in the construction of memory kernels of mesoscopic colloidal dynamics based on molecular dynamics trajectories.

■ ASSOCIATED CONTENT

Supporting Information

The Supporting Information is available free of charge at https://pubs.acs.org/doi/10.1021/acs.jpcb.2c06035.

Numerical details of the simulation results; values for the pressure correction term; statistical analysis of the temperature distribution width; histogram of instantaneous temperature of TIPS3P water simulation, and cumulative integrals of discussed autocorrelation functions (PDF)

■ AUTHOR INFORMATION

Corresponding Author

Peter Klein − *Fraunhofer ITWM, 67663 Kaiserslautern, Germany*; orcid.org/0000-0002-5468-8889; Email: peter.klein@itwm.fraunhofer.de

Authors

René Hafner − *Fraunhofer ITWM, 67663 Kaiserslautern, Germany; Physics Department and Research Center OPTIMAS, University Kaiserslautern, 67663 Kaiserslautern, Germany*; orcid.org/0000-0003-3683-662X

Gabriela Guevara-Carrion − *Thermodynamics and Process Engineering, Technische Universität Berlin, 10587 Berlin, Germany*

Jadran Vrabec − *Thermodynamics and Process Engineering, Technische Universität Berlin, 10587 Berlin, Germany*; orcid.org/0000-0002-7947-4051

Complete contact information is available at: https://pubs.acs.org/10.1021/acs.jpcb.2c06035

Notes

The authors declare no competing financial interest.

The data that support the findings of this study are available from the corresponding author upon reasonable request.

■ ACKNOWLEDGMENTS

R.H. and P.K. acknowledge support by the Fraunhofer Internal Programs under Grant Nr. MEF 835 617. R.H. gladly acknowledges supercomputer time on the Elwetritsch cluster at RHRK of TU Kaiserslautern, as well as on the Beehive cluster of the Fraunhofer ITWM. The authors G.G.-C. and J.V. acknowledge the financial support of the DFG under the grant VR 6/11. ms2 simulations were performed on the HPE Apollo system Hawk at the High Performance Computing Centre Stuttgart (HLRS) contributing to the project MMHBF2.

■ REFERENCES

(1) Braun, E.; Moosavi, S. M.; Smit, B. Anomalous Effects of Velocity Rescaling Algorithms: The Flying Ice Cube Effect Revisited. *J. Chem. Theory Comput.* **2018**, *14*, 5262−5272.

(2) Woodcock, L. V. Isothermal molecular dynamics calculations for liquid salts. *Chem. Phys. Lett.* **1971**, *10*, 257−261.

(3) Andersen, H. C. Molecular dynamics simulations at constant pressure and/or temperature. *J. Chem. Phys.* **1980**, *72*, 2384−2393.

(4) Nosé, S. A molecular dynamics method for simulations in the canonical ensemble. *Mol. Phys.* **1984**, *52*, 255−268.

(5) Berendsen, H. J. C.; Postma, J. P. M.; van Gunsteren, W. F.; DiNola, A.; Haak, J. R. Molecular dynamics with coupling to an external bath. *J. Chem. Phys.* **1984**, *81*, 3684−3690.

(6) Bussi, G.; Donadio, D.; Parrinello, M. Canonical sampling through velocity rescaling. *J. Chem. Phys.* **2007**, *126*, No. 014101.

(7) Basconi, J. E.; Shirts, M. R. Effects of Temperature Control Algorithms on Transport Properties and Kinetics in Molecular Dynamics Simulations. *J. Chem. Theory Comput.* **2013**, *9*, 2887−2899.

(8) Leimkuhler, B.; Noorizadeh, E.; Penrose, O. Comparing the Efficiencies of Stochastic Isothermal Molecular Dynamics Methods. *J. Stat. Phys.* **2011**, *143*, 921−942.

(9) Landau, L. D.; Lifshitz, E. M.*Fluid Mechanics*, 2nd ed.; Pergamon, 1987; Vol. *6*.

(10) Stokes, G. G.*Mathematical and Physical Papers*; Cambridge University Press, 2009; Vol. *1*, pp 75−129.

(11) Garrett, S. L.*Understanding Acoustics*; Springer International Publishing: Cham, 2020.

(12) Hall, L. The Origin of Ultrasonic Absorption in Water. *Phys. Rev.* **1948**, *73*, 775−781.

(13) Boukharfane, R.; Ferrer, P. J. M.; Mura, A.; Giovangigli, V. On the role of bulk viscosity in compressible reactive shear layer developments. *Eur. J. Mech. - B/Fluids* **2019**, *77*, 32−47.
(14) Klippenstein, V.; van der Vegt, N. F. A. Cross-correlation corrected friction in (generalized) Langevin models. *J. Chem. Phys.* **2021**, *154*, No. 191102.
(15) Jung, G.; Hanke, M.; Schmid, F. Iterative Reconstruction of Memory Kernels. *J. Chem. Theory Comput.* **2017**, *13*, 2481−2488.
(16) Antlinger, H.; Beigelbeck, R.; Clara, S.; Cerimovic, S.; Keplinger, F.; Jakoby, B. Investigation and Modeling of an Acoustoelectric Sensor Setup for the Determination of the Longitudinal Viscosity. *IEEE Trans. Ultrason., Ferroelect., Freq. Control* **2016**, *63*, 2187−2197.
(17) Holmes, M. J.; Parker, N. G.; Povey, M. J. W. Temperature dependence of bulk viscosity in water using acoustic spectroscopy. *J. Phys.: Conf. Ser.* **2011**, *269*, No. 012011.
(18) Mori, H. Collective Motion of Particles at Finite Temperatures. *Prog. Theor. Phys.* **1962**, *28*, 763−783.
(19) Mori, H. Transport, Collective Motion, and Brownian Motion. *Prog. Theor. Phys.* **1965**, *33*, 423−455.
(20) Hoheisel, C.; Vogelsang, R.; Schoen, M. Bulk viscosity of the Lennard-Jones fluid for a wide range of states computed by equilibrium molecular dynamics. *J. Chem. Phys.* **1987**, *87*, 7195−7198.
(21) Hess, B. Determining the shear viscosity of model liquids from molecular dynamics simulations. *Chem. Phys. Lett.* **2002**, *116*, No. 209.
(22) Kalibaeva, G.; Ferrario, M.; Ciccotti, G. Constant pressure-constant temperature molecular dynamics: a correct constrained NPT ensemble using the molecular virial. *Mol. Phys.* **2003**, *101*, 765−778.
(23) McQuarrie, D. A.*Statistical Mechanics*; University Science Books: Sausalito, Calif. and Great Britain, 2000.
(24) Zwanzig, R. Time-Correlation Functions and Transport Coefficients in Statistical Mechanics. *Annu. Rev. Phys. Chem.* **1965**, *16*, 67−102.
(25) Allen, M. P.; Tildesley, D. J.*Computer Simulation of Liquids*, 2nd ed.; Oxford University Press: Oxford, 2017.
(26) Allen, M. P. Atomic and molecular representations of molecular hydrodynamic variables. *Mol. Phys.* **1984**, *52*, 705−716.
(27) Percival, D. B. Three Curious Properties of the Sample Variance and Autocovariance for Stationary Processes with Unknown Mean. *Am. Stat.* **1993**, *47*, 274−276.
(28) Fuller, W. A.*Introduction to Statistical Time Series*, 2nd ed.; J. Wiley: New York and Chichester, 1996.
(29) van der Spoel, D.; van Maaren, P. J.; Berendsen, H. J. C. A systematic study of water models for molecular simulation: Derivation of water models optimized for use with a reaction field. *J. Chem. Phys.* **1998**, *108*, 10220−10230.
(30) Gowers, R. J.; Carbone, P. A multiscale approach to model hydrogen bonding: The case of polyamide. *J. Chem. Phys.* **2015**, *142*, No. 224907.
(31) van der Spoel, D.; Lindahl, E.; Hess, B.; Groenhof, G.; Mark, A. E.; Berendsen, H. J. C. GROMACS: fast, flexible, and free. *J. Comput. Chem.* **2005**, *26*, 1701−1718.
(32) Lindahl, E.; Abraham, M. J.; Hess, B.; van der Spoel, D.*GROMACS 2021.2 Manual*2021.
(33) Michaud-Agrawal, N.; Denning, E. J.; Woolf, T. B.; Beckstein, O. MDAnalysis: a toolkit for the analysis of molecular dynamics simulations. *J. Comput. Chem.* **2011**, *32*, 2319−2327.
(34) Gowers, R.; Linke, M.; Barnoud, J.; Reddy, T.; Melo, M.; Seyler, S.; Domański, J.; Dotson, D.; Buchoux, S.; Kenney, I.; Beckstein, O.. *MDAnalysis: A Python Package for the Rapid Analysis of Molecular Dynamics Simulations*; Proceedings of the Python in Science Conference, 2016.
(35) Phillips, J. C.; Hardy, D. J.; Maia, J. D. C.; Stone, J. E.; Ribeiro, J. V.; Bernardi, R. C.; Buch, R.; Fiorin, G.; Hénin, J.; Jiang, W.; et al. Scalable molecular dynamics on CPU and GPU architectures with NAMD. *J. Chem. Phys.* **2020**, *153*, No. 044130.
(36) Abraham, M. J.; Murtola, T.; Schulz, R.; Páll, S.; Smith, J. C.; Hess, B.; Lindahl, E. GROMACS: High performance molecular simulations through multi-level parallelism from laptops to supercomputers. *SoftwareX* **2015**, *1−2*, 19−25.
(37) Berendsen, H.; van der Spoel, D.; van Drunen, R. GROMACS: A message-passing parallel molecular dynamics implementation. *Comput. Phys. Commun.* **1995**, *91*, 43−56.
(38) Hess, B.; Kutzner, C.; van der Spoel, D.; Lindahl, E. GROMACS 4: Algorithms for Highly Efficient, Load-Balanced, and Scalable Molecular Simulation. *J. Chem. Theory Comput.* **2008**, *4*, 435−447.
(39) Lindahl, E.; Hess, B.; van der Spoel, D. GROMACS 3.0: a package for molecular simulation and trajectory analysis. *J. Mol. Model.* **2001**, *7*, 306−317.
(40) Páll, S.; Abraham, M. J.; Kutzner, C.; Hess, B.; Lindahl, E.*Solving Software Challenges for Exascale*; Markidis, S.; Laure, E., Eds.; Springer International Publishing: Cham, 2015; Vol. *8759*, pp 3−27.
(41) Pronk, S.; Páll, S.; Schulz, R.; Larsson, P.; Bjelkmar, P.; Apostolov, R.; Shirts, M. R.; Smith, J. C.; Kasson, P. M.; van der Spoel, D.; Hess, B.; Lindahl, E. GROMACS 4.5: a high-throughput and highly parallel open source molecular simulation toolkit. *Bioinformatics* **2013**, *29*, 845−854.
(42) Rutkai, G.; Köster, A.; Guevara-Carrion, G.; Janzen, T.; Schappals, M.; Glass, C. W.; Bernreuther, M.; Wafai, A.; Stephan, S.; Kohns, M.; et al. ms2: A molecular simulation tool for thermodynamic properties, release 3.0. *Comput. Phys. Commun.* **2017**, *221*, 343−351.
(43) Fingerhut, R.; Guevara-Carrion, G.; Nitzke, I.; Saric, D.; Marx, J.; Langenbach, K.; Prokopev, S.; Celný, D.; Bernreuther, M.; Stephan, S.; et al. ms2: A molecular simulation tool for thermodynamic properties, release 4.0. *Comput. Phys. Commun.* **2021**, *262*, No. 107860.
(44) NAMD User's Guide. 2021; https://www.ks.uiuc.edu/Research/namd/cvs/ug.pdf, (accessed 2021-11-10).
(45) In Gromacs, Bussi's thermostat is named velocity rescaling.
(46) Zwanzig, R.*Nonequilibrium Statistical Mechanics*; Oxford University Press: Oxford, 2001.
(47) Martyna, G. J.; Klein, M. L.; Tuckerman, M. Nosé−Hoover chains: The canonical ensemble via continuous dynamics. *J. Chem. Phys.* **1992**, *97*, 2635−2643.
(48) MacKerell, A. D.; Bashford, D.; Bellott, M.; Dunbrack, R. L.; Evanseck, J. D.; Field, M. J.; Fischer, S.; Gao, J.; Guo, H.; Ha, S.; et al. All-atom empirical potential for molecular modeling and dynamics studies of proteins. *J. Phys. Chem. B* **1998**, *102*, 3586−3616.
(49) Abascal, J. L. F.; Vega, C. A general purpose model for the condensed phases of water: TIP4P/2005. *J. Chem. Phys.* **2005**, *123*, No. 234505.
(50) Jorgensen, W. L.; Chandrasekhar, J.; Madura, J. D.; Impey, R. W.; Klein, M. L. Comparison of simple potential functions for simulating liquid water. *J. Chem. Phys.* **1983**, *79*, 926−935.
(51) http://catalan.quim.ucm.es/, (accessed 2021-11-10).
(52) Martyna, G. J.; Tobias, D. J.; Klein, M. L. Constant pressure molecular dynamics algorithms. *J. Chem. Phys.* **1994**, *101*, 4177−4189.
(53) Feller, S. E.; Zhang, Y.; Pastor, R. W.; Brooks, B. R. Constant pressure molecular dynamics simulation: The Langevin piston method. *Mol. Phys.* **1995**, *103*, 4613−4621.
(54) Yeh, I.-C.; Hummer, G. System-Size Dependence of Diffusion Coefficients and Viscosities from Molecular Dynamics Simulations with Periodic Boundary Conditions. *J. Phys. Chem. B* **2004**, *108*, 15873−15879.
(55) their simulation volume was 50% smaller than then present one.
(56) Fanourgakis, G. S.; Medina, J. S.; Prosmiti, R. Determining the bulk viscosity of rigid water models. *J. Phys. Chem. A* **2012**, *116*, 2564−2570.
(57) González, M. A.; Abascal, J. L. F. The shear viscosity of rigid water models. *J. Chem. Phys.* **2010**, *132*, No. 096101.
(58) Guevara-Carrion, G.; Vrabec, J.; Hasse, H. Prediction of self-diffusion coefficient and shear viscosity of water and its binary mixtures with methanol and ethanol by molecular simulation. *J. Chem. Phys.* **2011**, *134*, No. 074508.

https://doi.org/10.1021/acs.jpcb.2c06035
J. Phys. Chem. B 2022, 126, 10172−10184

(59) Tazi, S.; Botan, A.; Salanne, M.; Marry, V.; Turq, P.; Rotenberg, B. Diffusion coefficient and shear viscosity of rigid water models. *J. Phys.: Condens. Matter* **2012**, *24*, No. 284117.
(60) Lee, S. H.; Kim, J. Transport properties of bulk water at 243-550 K: a Comparative molecular dynamics simulation study using SPC/E, TIP4P, and TIP4P/2005 water models. *Mol. Phys.* **2019**, *117*, 1926−1933.
(61) Wu, Y.; Tepper, H. L.; Voth, G. A. Flexible simple point-charge water model with improved liquid-state properties. *J. Chem. Phys.* **2006**, *124*, No. 024503.
(62) Balasubramanian, S.; Mundy, C. J.; Klein, M. L. Shear viscosity of polar fluids: Molecular dynamics calculations of water. *Mol. Phys.* **1996**, *105*, 11190−11195.
(63) Mao, Y.; Zhang, Y. Thermal conductivity, shear viscosity and specific heat of rigid water models. *Chem. Phys. Lett.* **2012**, *542*, 37−41.
(64) Ong, E. E.; Liow, J.-L. The temperature-dependent structure, hydrogen bonding and other related dynamic properties of the standard TIP3P and CHARMM-modified TIP3P water models. *Fluid Phase Equilib.* **2019**, *481*, 55−65.
(65) Venable, R. M.; Hatcher, E.; Guvench, O.; Mackerell, A. D.; Pastor, R. W. Comparing simulated and experimental translation and rotation constants: range of validity for viscosity scaling. *J. Phys. Chem. B* **2010**, *114*, 12501−12507.
(66) Song, Y.; Dai, L. L. The shear viscosities of common water models by non-equilibrium molecular dynamics simulations. *Mol. Simul.* **2010**, *36*, 560−567.
(67) Braun, D.; Boresch, S.; Steinhauser, O. Transport and dielectric properties of water and the influence of coarse-graining: comparing BMW, SPC/E, and TIP3P models. *J. Chem. Phys.* **2014**, *140*, No. 064107.
(68) Lebowitz, J. L.; Percus, J. K.; Verlet, L. Ensemble Dependence of Fluctuations with Application to Machine Computations. *Phys. Rev.* **1967**, *153*, 250−254.
(69) Frenkel, D.; Smit, B.; Ratner, M. A. Understanding Molecular Simulation: From Algorithms to Applications. *Phys. Today* **1997**, *50*, No. 66.
(70) Mattingly, J. C.; Stuart, A. M.; Higham, D. J. Ergodicity for SDEs and approximations: locally Lipschitz vector fields and degenerate noise. *Stochastic Process. Appl.* **2002**, *101*, 185−232.
(71) Bussi, G.; Parrinello, M. Stochastic thermostats: comparison of local and global schemes. *Comput. Phys. Commun.* **2008**, *179*, 26−29.
(72) Bandyopadhyay, S.; Chakraborty, S.; Bagchi, B. Secondary structure sensitivity of hydrogen bond lifetime dynamics in the protein hydration layer. *J. Am. Chem. Soc.* **2005**, *127*, 16660−16667.
(73) Finkelstein, J.; Fiorin, G.; Seibold, B. Comparison of modern Langevin integrators for simulations of coarse-grained polymer melts. *Mol. Phys.* **2020**, *118*, No. e1649493.
(74) Goga, N.; Rzepiela, A. J.; de Vries, A. H.; Marrink, S. J.; Berendsen, H. J. C. Efficient Algorithms for Langevin and DPD Dynamics. *J. Chem. Theory Comput.* **2012**, *8*, 3637−3649.
(75) Schappals, M.; Mecklenfeld, A.; Kröger, L.; Botan, V.; Köster, A.; Stephan, S.; García, E. J.; Rutkai, G.; Raabe, G.; Klein, P.; et al. Round Robin Study: Molecular Simulation of Thermodynamic Properties from Models with Internal Degrees of Freedom. *J. Chem. Theory Comput.* **2017**, *13*, 4270−4280.

https://doi.org/10.1021/acs.jpcb.2c06035
J. Phys. Chem. B 2022, 126, 10172−10184